Applied Physics Letters

RESEARCH ARTICLE | JULY 31 2024

Raman spectroscopy capabilities for advanced semiconductor technology devices

Thomas Nuytten ; Janusz Bogdanowicz ; Stefanie Sergeant ; Claudia Fleischmann

Appl. Phys. Lett. 125, 053506 (2024)
https://doi.org/10.1063/5.0219438

Articles You May Be Interested In

Controllable carrier transfer modulation of ambipolar van der Waals semiconductors toward forksheet FETs

Appl. Phys. Lett. (May 2024)

Critical need and future directions of SIMS depth profiling in CMOS fabrication

J. Vac. Sci. Technol. B (January 2018)

Uncertainty in linewidth quantification of overlapping Raman bands

Rev. Sci. Instrum. (January 2019)

23 June 2025 13:30:16

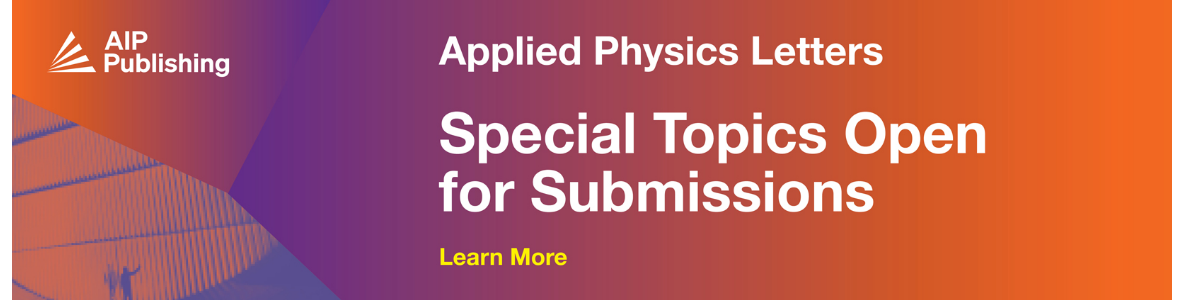

Applied Physics Letters ARTICLE pubs.aip.org/aip/apl

Raman spectroscopy capabilities for advanced semiconductor technology devices

Cite as: Appl. Phys. Lett. **125**, 053506 (2024); doi: 10.1063/5.0219438
Submitted: 17 May 2024 · Accepted: 21 July 2024 ·
Published Online: 31 July 2024

Thomas Nuytten,[1,a)] Janusz Bogdanowicz,[1] Stefanie Sergeant,[1] and Claudia Fleischmann[1,2]

AFFILIATIONS

[1]IMEC, Kapeldreef 75, B-3001 Leuven, Belgium
[2]KU Leuven, Department of Physics and Astronomy, Quantum Solid-State Physics, Celestijnenlaan 200D, B-3001 Leuven, Belgium

[a)]Author to whom correspondence should be addressed: thomas.nuytten@imec.be

ABSTRACT

In semiconductor processing and metrology, Raman spectroscopy is a valuable characterization tool because of its nondestructive nature, high throughput, and versatility in terms of parameter sensitivity. However, with the miniaturization of semiconductor devices, the inherent diffraction limit of the optical technique becomes a roadblock. In order to re-enable the strengths of Raman spectroscopy at the nanometer scale, we exploit polarization-induced enhancement effects that focus the excitation light into the region of interest, without the need for external probes or particles. This allows the detection of structures with dimensions far smaller than the excitation wavelength, unlocking the strengths of Raman spectroscopy at the nanoscale for, e.g., stress and composition measurements. Moreover, under these conditions the experiment probes the totality of the materials stack and we show how this transforms the technique into a volumetric and geometric measurement. The result is a completely new application domain for Raman spectroscopy as a critical dimensional metrology toolkit for a wide variety of semiconducting and metallic materials.

© 2024 Author(s). All article content, except where otherwise noted, is licensed under a Creative Commons Attribution-NonCommercial-NoDerivs 4.0 International (CC BY-NC-ND) license (https://creativecommons.org/licenses/by-nc-nd/4.0/). https://doi.org/10.1063/5.0219438

23 June 2025 13:30:16

Raman spectroscopy is a very versatile technique with sensitivity to, e.g., mechanical stress, composition, and doping, while still being noninvasive and fast.[1–4] Photoluminescence (PL) has a similar application space and will often provide complementary information to that of Raman spectroscopy, and since there is considerable overlap in the required hardware, the techniques are frequently used together. While the concepts proposed in this paper will be applicable to both techniques, we will focus the discussion on applications of Raman spectroscopy. However, as optical spectroscopic methods they are both inherently diffraction-limited. In order to re-enable the strengths of Raman spectroscopy and PL at the nanometer scale, we make use of a polarization-induced enhancement effect that boosts the sensitivity to sub-wavelength dimensions while simultaneously extending the application domain of Raman analysis into dimensional metrology.

In a standard micro-Raman spectroscopic arrangement, the excitation light is focused onto the sample using a microscope objective that limits the spatial resolution to dimensions of the order of the (usually visible) wavelength. Moreover, the penetration depth of the light, which depends on the material under study and the excitation wavelength, is typically of the same order, meaning that the total probed volume is very large compared to modern nano-electronics dimensions and transistor channels of typically only a few tens of nanometer. At the same time, semiconductor devices are virtually always patterned in grating-like, periodic structures that have widths and pitches of similar dimensions (tens to hundreds of nanometers), again much smaller than the laser spot. However, when aligning the linear polarization of the excitation laser with the structure geometry, the description of the coupling of the light into the structures is dramatically different from that of bulk material.[5–7] Through finite element simulations and band structure calculations, it was found in previous studies that the grating-like structure acts as a photonic crystal, which leads to confinement of the available modes for transmission into the material of interest under the right experimental conditions.[8,9] As the optical beam is effectively guided into the nanostructured lines, an enhancement of the signal from this region of interest over orders of magnitude is achieved, and the Raman spectrum becomes dominated by the response of just a tiny fraction of the total probed volume. Indeed, using grating samples with about 10% areal coverage and given the penetration depth of visible laser light in the materials under study (∼140 nm for 405 nm in Si), the active region represents only ∼2% of the total material volume under the incident beam. The degree of enhancement is the result of an interplay between the excitation

© Author(s) 2024

wavelength and the material, dimension, and pitch of the grating,[8] but is preserved even for a single illuminated fin,[7] meaning that under these so-called nano-focusing conditions, the Raman scattering originating from the material under study becomes strong enough to enable detailed analysis. It is important to emphasize that in order to achieve this effect, no external apparatus modification or sample preparation is required, the enhancement is obtained simply by observing a correct arrangement of incident polarization and structure alignment. As such, characterization of for instance mechanical stress and composition becomes possible on structures with dimensions far beyond the diffraction limit.

The results presented in this paper were obtained using a Horiba Scientific LabRAM HR spectrometer equipped with 405, 532, 633, and 785 nm excitation lasers in backscattering geometry. Unless specified otherwise, the 405 nm laser was used for excitation, which thanks to the penetration depth of only ∼140 nm in Si has the highest surface sensitivity. Other excitation wavelengths remain available if, depending on the material's absorption and thickness, different penetration depths are required. The integration time was 60 s, which for a typical full 300 mm wafer characterization at 25 different locations would result in about half an hour of measurement time. Diffraction gratings of 1800 or 2400 g/mm were selected depending on the required spectral resolution or throughput, and the laser light was focused onto the sample by a 100× 0.9NA objective, resulting in a spot size slightly below 1 μm. This tight focus results in a laser power density of around 160 kW/cm^2, which may result in moderate heating-induced peak shifts (<1 cm^{-1}), which are not considered here since we work with relative peak intensities exclusively. The polarization from the linearly polarized, solid-state laser source was adjusted using a $\lambda/2$ waveplate followed by a polarizer optic (linear polarizer) for precise control of the incident polarization, which is critical in these experiments.

With the electric field confined to the small nanostructures under investigation, the penetration depth of the light is still heavily dependent on the wavelength of the selected excitation source. The total penetration depth may extend into the micrometer range, and is much larger than the typical thickness of the device channels, meaning that the totality of the channel volume is probed, often together with a considerable portion of the substrate used for the fabrication of the structures. Since the complete stack is being probed by the incident laser, the intensity of the collected Raman scattering scales with the total volume of the structure. Therefore, when normalizing the signal from such channels to another reference signal in the spectrum (like Si–Si scattering from the substrate), we obtain a volumetric measurement of the amount of material present in the probed volume. As a demonstration of this concept, Fig. 1 shows the Raman spectrum of a 100 nm-wide fin consisting of an alternating stack of $Si_{75}Ge_{25}$ and Si layers, grown on top of a Si substrate, with a pitch of 420 nm, and composition verified by x-ray diffraction (not shown). The Raman spectrum then reveals two contributions of Si–Si scattering, one originating from the SiGe layers at lower wavenumber, and one originating from the Si layers and the Si substrate combined, appearing around the typical crystalline Si (cSi) Raman frequency of 520 cm^{-1}. The relative contribution of the substrate and Si nanosheets will depend on the chosen wavelength as well as the thickness and the composition of the stack, and any potential residual strain in the nanosheets will broaden or shift the peak away from the unstrained peak position. While in general the Raman intensity is only a qualitative parameter that depends on

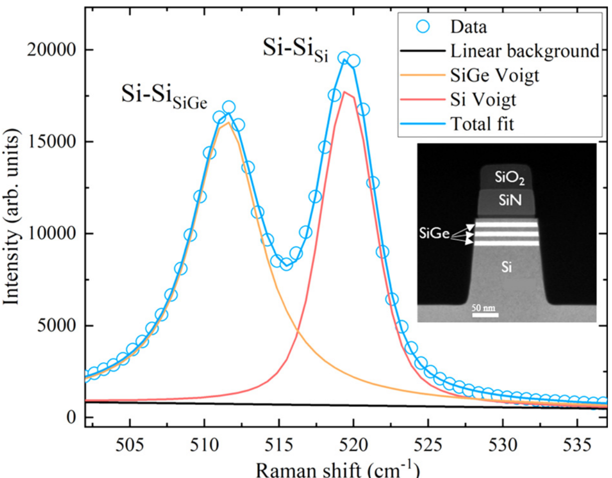

FIG. 1. High spectral resolution Raman spectrum of a stacked semiconductor device containing alternating Si and $Si_{75}Ge_{25}$ layers. We observe both Si- and SiGe-related Si–Si vibrations and can analyze these signals independently. The inset shows a cross section profile of the structure obtained by high-angle annular dark-field scanning tunneling electron microscopy (HAADF STEM), where the alternating stack of SiGe and Si layers is visible.

experimental and environmental conditions, here the peak around 510 cm^{-1} is a probe for the total amount of SiGe present in the stack, while simultaneously carrying an internal reference signal from Si layers that are unaffected by following processing steps, at 520 cm^{-1}. We will clarify this concept in a couple of examples, demonstrating how this approach opens a completely new application domain for Raman spectroscopy as a dimensional measurement.

First, in gate-all-around field-effect transistors (GAA FETs[10]), a metrology challenge emerges as the SiGe in the Si/$Si_{75}Ge_{25}$ stack [see inset micrograph of Fig. 2(a)] is etched selectively from the sides, revealing the Si transistor channel for further processing. The depth of that cavity is an important parameter to control but is virtually inaccessible using the standard characterization techniques for profilometric measurements, making its measurement a challenge for most top-down techniques such as critical dimension-scanning electron microscopy (CD-SEM).[11] We use the Raman scattering coming from the SiGe layer and normalize that to the Si–Si scattering that is collected from the Si layers in between the SiGe and the Si substrate combined, both of whose material volumes remain unchanged during the etch. When carrying out this analysis on a selection of three different etch depths, we can see from panel (a) in Fig. 2 that the normalized integrated intensity of the Raman signal decreases uniformly as the cavity depth increases. Moreover, the sensitivity of this parameter equals that of a true volumetric measurement through transmission electron microscopy (TEM), as the trend follows the ratio of the normalized remaining volume of SiGe (V/V_0, dashed line in the plot).

Second, a similar metrology challenge exists in 3D memory technology employing polycrystalline Si (PolySi) in, e.g., 3DNAND stacks. The characterization of the depth of an etch process will be impossible through most spectroscopic techniques, as there is usually no means to differentiate between different phases of the same material, in this case Si. Here, we rely on the slight offset of Si–Si Raman scattering in PolySi with respect to that of cSi to measure the etch depth of the cavity that

23 June 2025 13:30:16

© Author(s) 2024

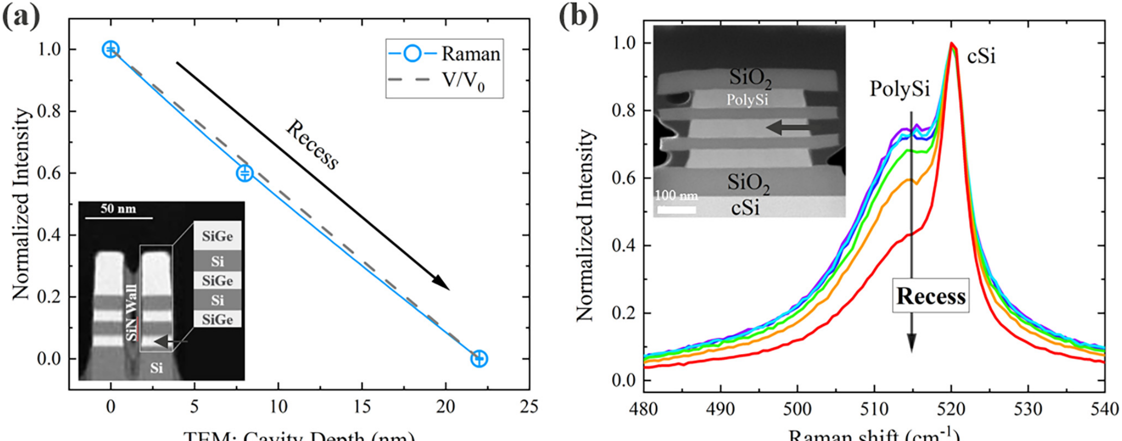

FIG. 2. (a) Normalized integrated intensity of the Si–Si vibration coming from $Si_{75}Ge_{25}$ to the Si–Si vibration coming from Si, as a function of the cavity depth as measured by TEM. As the recess progresses (see black arrow in the TEM micrograph of the unetched structure), the profile follows the nominal remaining volume of SiGe (V/V_0, dashed line). (b) Spectra of a collection of samples with increasing PolySi etch quantities plotted normalized to the Si background. The PolySi shoulder clearly decreases with increasing etch. The inset shows a HAADF STEM image of the structure under study with alternating PolySi and SiO_2 layers.

originates as the PolySi is etched between the SiO_2 in the stack [see inset of Fig. 2(b)]. The typical signal for PolySi appears in the spectrum about $5\,cm^{-1}$ below the characteristic peak of cSi from the substrate, and equipment with sufficient spectral resolution will be able to clearly distinguish this signal from a cSi background. Similarly as with the SiGe etch, we have a selection of samples where the cavity depth progresses in the sample set, and it can be seen in panel (b) of Fig. 2 that when we normalize the spectra to the cSi background from the substrate, the characteristic PolySi signal at slightly lower wavenumber decreases significantly. The ratio of this intensity to the cSi background can be used as a quantitative measure of the remaining volume of PolySi and hence of the depth of the cavity. It was indeed confirmed by TEM measurements that there is a 1-on-1 relationship between the normalized PolySi Raman intensity and the depth of the etched cavity (not shown here).

Third, it was found that the application of the effect is not limited to Raman-active materials but that it can be used for, e.g., metal lines as well. In this case, we need to align the incident polarization perpendicularly to the metal lines such that now the excitation light is confined into the region in between the lines,[8] which is filled with an oxide like SiO_2. This enables the light to reach the underlying Si substrate, and the Raman signal detected comes from the substrate but crucially carries information on the critical dimension (CD) of the metal lines it has passed. When studying a collection of for instance TiN lines with varying CD but fixed line pitch of 32 nm, we see a strong correlation between the normalized Raman intensity from the substrate and the width of the lines (see Fig. 3). The datapoint at 0 nm CD corresponds to a reference measurement on bulk Si, where effectively no superimposed metal grating modulates the backscattered Raman signal. Interestingly, the sensitivity of the measurement becomes stronger as we move to longer excitation wavelengths as is demonstrated by a slope of the linear fit that increases as the wavelength of the excitation light increases. This is explained through the light–matter interaction that takes place in the photonic crystal, where the transmission through the metal grating (and hence the returning Si Raman signal) is governed by the effective extinction coefficient κ_{eff}, which in these systems increases with increasing wavelength. Aided by finite element simulations, Gawlik *et al.* then developed an analytical model that shows that a stronger extinction (larger κ_{eff} at longer wavelength) leads to a higher sensitivity.[12] When the metals involved would enable plasmonic enhancement as well, we foresee that these effects could co-exist to obtain a hybrid and multi-mode enhancement scheme as was observed in other systems before.[13,14]

Finally, the true selectivity of the optimization can be demonstrated using samples that have been processed both trough fin and subsequent replacement gate definition. Therefore, we use forksheet

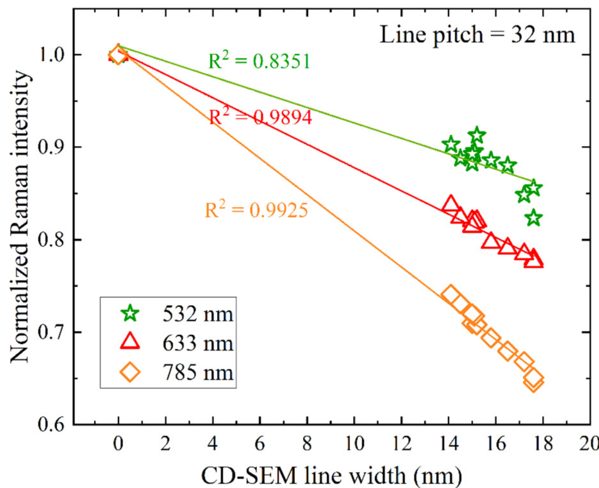

FIG. 3. Normalized Raman intensity from a TiN grating with underlying Si as a function of the TiN linewidth as measured by CD-SEM. The technique is able to capture tiny variations in CD with a sensitivity that increases with increasing wavelength of the probing laser. Two samples for the largest linewidth were available and are included in the graph.

23 June 2025 13:30:16

© Author(s) 2024

transistor architectures after replacement gate processing, characterized by two gratings of first the n and p metal-oxide-semiconductor (MOS) transistor structures and then subsequently 150–200 nm-thick amorphous Si (aSi) lines, with both gratings orthogonal to each other. The transistor structures again consist of an alternating stack of Si and $Si_{75}Ge_{25}$ layers where along the different samples the SiGe is progressively etched away from between the Si. When we align the incident polarization of the 405 nm excitation laser to the fin geometry, we record Raman spectra that carry the information from the SiGe and Si material of the fin, and the aSi does not pollute the spectra [see Fig. 4(a)]. When studying three different samples with respectively no etch, an 8 nm-deep etch, and fully etched SiGe, we retain the progressive disappearance of the SiGe-related signals as was described in, e.g., Fig. 2(a). Indeed, again the intensity of the Si–Si scattering as a shoulder to the main cSi peak and the Si–Ge related peaks[15] around 400 cm^{-1} clearly follow the trend of SiGe removal, and similarly as demonstrated earlier, we can extend this metrology to a quantitative measurement of the remaining SiGe. Strikingly, we can completely reverse the sensitivity of the experiment to the replacement gate material by simply rotating the incident polarization by 90°, now aligned with the grating formed by the aSi lines. This results in the spectrum shown in Fig. 4(b), where the Si and SiGe features have completely disappeared, and only the characteristic vibration around 480 cm^{-1} from aSi is observed. The processing steps that make up the parameter split of the three samples under study here do not attack the aSi, therefore as expected we see an unaltered aSi intensity throughout the sample split, with very good repeatability. We note that for these experiments in particular, it is critical to use first a $\lambda/2$ waveplate to rotate the incident polarization, followed by a linear polarizer optic still in the incident path, to further purify the incident polarization selection. Indeed the Raman scattering efficiency of the fin materials patterned in the perpendicular direction is so strong that even the slightest misalignment will enable the cSi and/or SiGe to contribute to the spectrum. With this precise polarization control however, the end result is that a simple rotation of the incident polarization allows us to be fully selective to either of the two independent gratings, again bringing the Raman capabilities (e.g., mechanical stress, composition, doping) to the individual gratings independently.

While Raman and PL have always been very strong and versatile techniques, their application in semiconductor processing environments has always been relatively limited. The focus was on failure analysis and laboratory-based pathfinding,[16–19] and the continuous miniaturization of semiconductor structures posed an additional challenge for their wide integration.

The current developments hold the promise to re-introduce the techniques for advanced semiconductor structures based on two critical enablers.

First, the optimized polarization condition for the relative orientation with respect to the structure geometry brings all strengths of Raman to the nanoscale. Indeed only through the nanofocusing effect can we detect the nanometer-sized structures and can their material properties be extracted from the Raman spectra. When compared to unpatterned, blanket layers of the same composition, the obtained Raman intensity on patterned structures can be increased over orders of magnitude,[7] making the extraction of, e.g., peak position or FWHM much more precise. From these parameters, the classical strengths of Raman spectroscopy for, among others, stress and composition measurements remain applicable at nanoscale dimensions.[20–22] This crucially enables metrology on structures much smaller than the excitation wavelength without the need for any sample preparation or tip-based near field enhancement.

Second, because the nanofocusing effect depends so strongly on the dimensions of the nanostructure, the phenomenon can also be exploited to study the dimensions themselves, which is a prime component of semiconductor metrology. The obtained intensities scale directly with the probed volume on the nanoscale, and we have demonstrated nanometer sensitivity to, e.g., the width of semiconductor and metal lines. This is a completely new application domain for Raman spectroscopy, which will greatly strengthen the position of the technique in state-of-the-art semiconductor processing and measurement environments.

While the described capabilities will certainly strengthen the position of optical spectroscopy in the semiconductor metrology landscape, certain limitations of the approach can be identified. Despite the dramatic enhancement, the spatial resolution of the technique remains

23 June 2025 13:30:16

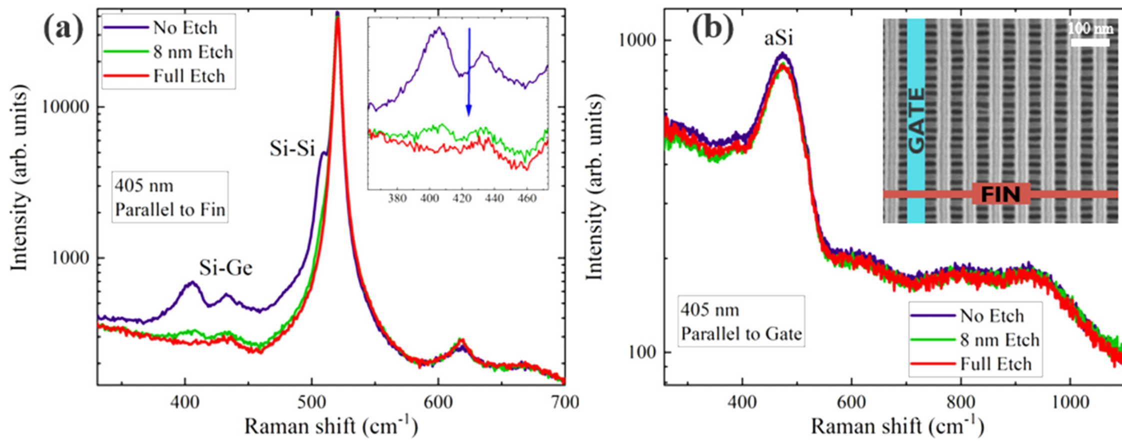

FIG. 4. (a) Raman spectra with polarization parallel to the fin structures. A strong sensitivity on remaining $Si_{75}Ge_{25}$ content is observed, and no aSi material from the replacement gate is detected. (b) Raman spectra recorded with now polarization parallel to the replacement gate. Only the aSi is observed in the spectra, and since this material is not subject to the etch process, the intensity is unaffected. The inset shows a top-down SEM image of the structures under investigation with gate and fin directions indicated.

© Author(s) 2024

unaltered and is still of the order of the excitation wavelength, implying that typically multiple structures will be probed at once in an ensemble measurement. Nonetheless, the Raman measurement remains a point-by-point operation, and many different measurement locations will be necessary to gather sufficient statistics. The same is true for the depth resolution, where based on the penetration depth of the laser light, several layers of the stack may be probed simultaneously. We estimate that an independent interrogation of the layers in a stack would require the use of several excitation wavelengths, combined with modeling efforts to disentangle the signals from the different layers.

In summary, these examples show that we have developed Raman spectroscopy into a dimensional metrology on industry-relevant structures, which in combination with the extensive set of applications for the technique re-enabled at the nanometer scale make it an essential toolkit in semiconductor manufacturing environments. We anticipate that these developments will find increasing application in high volume manufacturing as 300 mm-capable Raman and PL tools are being introduced into the semiconductor fabs.

The authors would like to acknowledge the imec programs for sample preparation and useful discussions.

AUTHOR DECLARATIONS

Conflict of Interest

The authors have no conflicts to disclose.

Author Contributions

Thomas Nuytten: Conceptualization (equal); Data curation (lead); Formal analysis (lead); Investigation (lead); Methodology (lead); Resources (equal); Writing – original draft (lead). **Janusz Bogdanowicz:** Conceptualization (equal); Formal analysis (supporting); Investigation (equal); Methodology (equal); Writing – review & editing (equal). **Stefanie Sergeant:** Data curation (equal); Investigation (equal). **Claudia Fleischmann:** Project administration (equal); Resources (equal); Writing – review & editing (equal).

DATA AVAILABILITY

The data that support the findings of this study are available from the corresponding author upon reasonable request.

REFERENCES

[1]I. De Wolf, J. Appl. Phys. **118**, 053101 (2015).
[2]S. Ganesan, A. A. Maradudin, and J. Oitmaa, Ann. Phys. **56**, 556 (1970).
[3]J. C. Tsang, P. M. Mooney, F. Dacol, and J. O. Chu, J. Appl. Phys. **75**, 8098 (1994).
[4]A. V. Baranov, A. V. Fedorov, T. S. Perova, R. A. Moore, V. Yam, D. Bouchier, V. L. Thanh, and K. Berwick, Phys. Rev. B **73**, 075322 (2006).
[5]V. Poborchii, T. Tada, and T. Kanayama, Appl. Phys. Lett. **94**, 131907 (2009).
[6]M. Kuhn, Y. Zhou, and K. Johnson, in The 2013 International Conference on Frontiers of Characterization and Metrology for Nanoelectronics (FCMN), Monterey, California, USA (2013).
[7]T. Nuytten, T. Hantschel, D. Kosemura, A. Schulze, I. De Wolf, and W. Vandervorst, Appl. Phys. Lett. **106**, 033107 (2015).
[8]J. Bogdanowicz, T. Nuytten, A. Gawlik, A. Schulze, I. De Wolf, and W. Vandervorst, Appl. Phys. Lett. **108**, 083106 (2016).
[9]J. Bogdanowicz, T. Nuytten, A. Gawlik, S. Sergeant, Y. Oniki, P. P. Gowda, H. Mertens, and A.-L. Charley, Nano Lett. **24**, 1191 (2024).
[10]H. Mertens, R. Ritzenthaler, Y. Oniki, B. T. Chan, B. Briggs, A. Hikavyy, T. Hopf, G. Mannaert, Z. Tao, F. Sebaai, A. Peter, K. Vandersmissen, E. Dupuy, E. Rosseel, D. Batuk, J. Geypen, G. T. Martinez, D. Abigail, E. Grieten, K. Dehave, J. Mitard, S. Subramanian, L.-A. Ragnarsson, P. Weckx, D. Jang, B. Chehab, G. Hellings, J. Ryckaert, E. D. Litta, and N. Horiguchi, in Symposium on VLSI Technology, T2-1-9:20 (2021).
[11]J. Bogdanowicz, Y. Oniki, K. Kenis, Y. Muraki, T. Nuytten, S. Sergeant, A. Franquet, V. Spampinato, T. Conard, I. Hoflijk, J. Meersschaut, N. Claessens, A. Moussa, D. Van Den Heuvel, J. Hung, R. Koret, A.-L. Charley, and P. Leray, in Proceedings of the SPIE 11611, Metrology, Inspection, and Process Control for Semiconductors Manufacturing XXXV, 116111Q (2021).
[12]A. Gawlik, J. Bogdanowicz, T. Nuytten, A.-L. Charley, L. Teugels, J. Misiewicz, and W. Vandervorst, Appl. Phys. Lett. **117**, 043102 (2020).
[13]C. P. T. McPolin, Y. N. Vila, A. V. Krasavin, J. Llorca, and A. V. Zayats, Nanophotonics **12**, 2997 (2023).
[14]A. Barreda, S. Hell, M. A. Weissflog, A. Minovich, T. Pertsch, and I. Staude, J. Quant. Spectrosc. Radiat. Transfer **276**, 107900 (2021).
[15]D. Rouchon, M. Mermoux, F. Bertin, and J. M. Hartmann, J. Cryst. Growth **392**, 66 (2014).
[16]V. Prabhakara, T. Nuytten, H. Bender, W. Vandervorst, S. Bals, and J. Verbeeck, Opt. Express **29**, 34531 (2021).
[17]Z. Khan, T. Nuytten, P. Favia, C. Fleischmann, I. De Wolf, and W. Vandervorst, J. Appl. Phys. **132**, 035104 (2022).
[18]P. Hermann, M. Hecker, D. Chumakov, M. Weisheit, J. Rinderknecht, A. Shelaev, P. Dorozhkin, and L. Eng, Ultramicroscopy **111**, 1630 (2011).
[19]G. Vanacore, M. Chaigneau, N. Barett, F. Boioli, M. Salvalaglio, F. Montalenti, N. Manini, L. Caramella, P. Biagioni, D. Chrastina, G. Isella, O. Renault, M. Zani, R. Sordan, G. Onida, R. Ossikovski, H.-J. Drouhin, and A. Tagliaferri, Phys. Rev. B **88**, 115309 (2013).
[20]D. Schmidt, C. Durfee, J. Li, N. Loubet, A. Cepler, L. Neeman, N. Meir, J. Ofek, Y. Oren, and D. Fishman, in Proceeding of the SPIE 11611, Metrology, Inspection, and Process Control for Semiconductor Manufacturing XXXV, 116111T (2021).
[21]I. De Wolf, V. Simons, S. A. Srinivasan, P. Verheyen, and R. Loo, ECS Trans. **86**, 397 (2018).
[22]T. Nuytten, J. Bogdanowicz, L. Witters, G. Eneman, T. Hantschel, A. Schulze, P. Favia, H. Bender, I. De Wolf, and W. Vandervorst, APL Mater. **6**, 058501 (2018).

23 June 2025 13:30:16

© Author(s) 2024